

# The effect of caesium on barium hollandites studied by neutron diffraction and magic-angle spinning (MAS) nuclear magnetic resonance

Karl R. Whittle · Sharon E. Ashbrook ·  
Gregory R. Lumpkin · Ian Farnan · Ronald I. Smith ·  
Simon A. T. Redfern

Received: 8 January 2007 / Accepted: 1 May 2007 / Published online: 20 July 2007  
© Springer Science+Business Media, LLC 2007

**Abstract** The structural effects of incorporating Cs into the monoclinic and tetragonal hollandites  $\text{Ba}_{1.2-x}\text{Cs}_x\text{Mg}_{1.2-x/2}\text{Ti}_{6.8+x/2}\text{O}_{16}$  and  $\text{Ba}_{1.2-x}\text{Cs}_x\text{Al}_{2.4-x}\text{Ti}_{5.6+x}\text{O}_{16}$  have been studied using powder neutron diffraction and  $^{133}\text{Cs}$  and  $^{27}\text{Al}$  MAS NMR. Addition of Cs to the monoclinic structure induces a ‘shear-type collapse’, in agreement with previously published results. NMR spectra show that the addition of Cs does not change the local structure around the Al cations within the tunnel walls. An algorithm is given that allows a prediction of unit cell parameters to be made for tetragonal hollandites containing barium.

## Introduction

Hollandite ( $\text{Ba}_2\text{Mn}_8\text{O}_{16}$ ) is a naturally occurring mineral that gives its name to a class of structures of stoichiometry  $\text{A}_2\text{B}_8\text{O}_{16}$  in which a framework of edge- and corner-sharing  $\text{BO}_6$  octahedra elongated tunnels in which the A cations are located in 8-fold coordination. The hollandite structure is versatile and can accommodate a variety of dopant atoms on both the A and B sites [1]—e.g., on the A site Ba, Na, Rb, Pb, Cs and K; on the B site it is possible to mix atoms such as Mo, Sn, Mg, Ti, Al, and Rh - to produce materials whose properties make them suitable for use in a variety of technological applications, examples of which are  $\text{Li}^+$  ionic conductors [2] and microwave dielectrics [3]. Recent studies have also been undertaken to determine the behaviour of hollandite at mid ocean ridges [4]. However, by far the biggest area of interest in hollandite lies in immobilisation of radioactive nuclides.

The use of nuclear power poses a number of questions particularly that of how to dispose of the resulting radioactive waste safely, with minimal affect on the biosphere. One of the more significant elements that needs to be immobilised safely is caesium, which has two radioactive isotopes;  $^{135}\text{Cs}$ , half-life ~2 million years, and  $^{137}\text{Cs}$ , ~30 years half-life. Both these Cs isotopes are  $\beta$ -emitters, which can result in high levels of radiogenic heating. One of the crystalline matrices of choice for immobilising both  $^{135}\text{Cs}$  and  $^{137}\text{Cs}$  is based on the hollandite-type systems  $\text{Ba}_{1.2-x}\text{Cs}_x\text{Mg}_{1.2-x/2}\text{Ti}_{6.8+x/2}\text{O}_{16}$  and  $\text{Ba}_{1.2-x}\text{Cs}_x\text{Al}_{2.4-x}\text{Ti}_{5.6+x}\text{O}_{16}$ .

In these systems the framework is built from  $\text{TiO}_6$  and  $\text{AlO}_6$  or  $\text{MgO}_6$  octahedra, with the A cations ( $\text{Ba}^{2+}$ ,  $\text{Cs}^+$ ) located within the tunnels (Fig. 1). Their crystal structures can be either monoclinic [5], e.g.,  $\text{Ba}_{1.2}\text{Mg}_{1.2}\text{Ti}_{6.8}\text{O}_{16}$ , or tetragonal [6], e.g.,  $\text{Ba}_{1.121}\text{Al}_{2.24}\text{Ti}_{5.76}\text{O}_{16}$ . Essentially the

K. R. Whittle · S. E. Ashbrook · G. R. Lumpkin ·  
I. Farnan · S. A. T. Redfern  
Department of Earth Sciences, Cambridge Centre for Ceramic  
Immobilisation, University of Cambridge, Downing Street,  
Cambridge CB2 3EQ, UK

K. R. Whittle (✉)  
Department of Engineering Materials, University of Sheffield,  
Mappin Street, Sheffield S1 3JD, UK  
e-mail: k.r.whittle@shef.ac.uk

*Present Address:*  
S. E. Ashbrook  
Department of Chemistry, University of St Andrews, North  
Haugh, St Andrews, Fife KY16 9ST, UK

*Present Address:*  
G. R. Lumpkin  
Australian Nuclear Science and Technology Organisation  
(ANSTO), PMB 1, Menai, NSW 2234, Australia

R. I. Smith  
ISIS Facility, Rutherford Appleton Laboratory, Chilton, Didcot,  
Oxfordshire OX11 0QX, UK

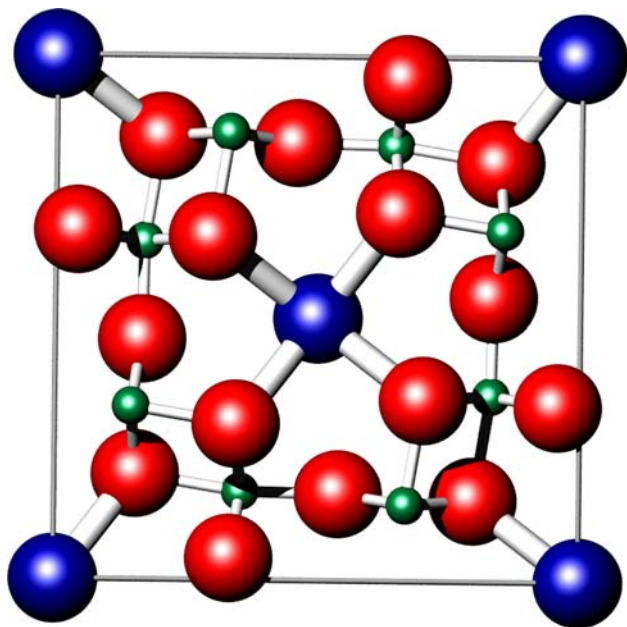


**Fig. 1** Image of a tetragonal hollandite [6], view looking down the c-axis, large black spheres are the A cations, small black spheres are the B cations, and large grey spheres are the O anions

difference is due to variations in A/B cation radius ratio, causing a shear-type collapse of the tunnel and a reduction in symmetry ( $I4/m \rightarrow C2/m$ ). It is reported that if  $R_B/R_A < 0.48$  then the structure is tetragonal, while for larger  $R_B/R_A$  a monoclinic structure forms [7]. Example crystal structures are shown in Table 1 and in Fig. 1 [5, 6].

In the area of nuclear waste immobilisation it is routine to base the hollandite on Ti, e.g.,  $Ba_{1.2}Mg_{1.2}Ti_{6.8}O_{16}$  [5]. The use of Ti is important, as once  $Cs^+$  undergoes  $\beta$ -decay forming  $Ba^{2+}$  a charge imbalance results. This imbalance is rectified if a  $Ti^{4+}$  cation in the lattice undergoes reduction to  $Ti^{3+}$ .

Candidate hollandites for immobilisation of Cs isotopes frequently contain  $Al^{3+}$  or  $Mg^{2+}$  species, which are added to ensure charge balance is maintained during synthesis, preventing the premature formation of  $Ti^{3+}$ . Such components are also used as they modify the tunnel size allowing the larger  $Cs^+$  cations to be accommodated on the A sites, e.g.,  $Cs^+ \sim 1.7 \text{ \AA}$  and  $Ba \sim 1.4 \text{ \AA}$ —both ions in 8-fold co-ordination.

Although, there is a broad understanding of where the cations are located in the tunnels, i.e.,  $Ba^{2+}/Cs^+$  locate there; the exact nature i.e., the ordering/periodicity is not well understood. Within the tunnels there are many sites that can be occupied, e.g., in  $Ba_{1.121}Al_{2.24}Ti_{5.76}O_{16}$  there are, formally, 4 Wyckoff sites available [6]. However, the nature of these sites preclude their complete occupancy, the average distance between the sites being less than the ionic diameter of  $Ba^{2+}$ . This implies a partial occupancy of these sites. Again using  $Ba_{1.121}Al_{2.24}Ti_{5.76}O_{16}$  as an example the fractional occupancy is 0.25.

Within the  $BO_6$  octahedra framework, cation mixing is often present, dependent on composition. However, the degree of mixing is dependent on the exact chemical composition and is normally random in nature, such that only a unit-cell average can be determined for the

**Table 1** Example unit cell information for two hollandites, 1 tetragonal [6] and 1 monoclinic [5]

Atom	Wyckoff site	X	Y	Z	Frac
$Ba_{1.12}Al_{2.24}Ti_{5.76}O_{16}$		$a = 9.9750 \text{ \AA}$	$b = 9.9750 \text{ \AA}$	$c = 2.92541 \text{ \AA}$	
		SPGR	$I4/m$		
Ba	4e	0	0	0.094	0.28
Ti	8h	0.3308	0.1454	0	0.72
Al	8h	0.3308	0.1454	0	0.28
O	8h	0.2982	0.3456	0	1
O	8h	0.0414	0.3344	0	1
$Ba_{1.14}Mg_{1.14}Ti_{6.86}O_{16}$		$a = 10.1816 \text{ \AA}$	$b = 2.97330 \text{ \AA}$	$c = 10.0268 \text{ \AA}$	
		SPGR	$C12/M1$		
Ba	4g	0	0.1	0	0.285
Mg	4i	0.3300	0	0.1513	0.1425
Ti	4i	0.3300	0	0.1513	0.8575
Mg	4i	0.8516	0	0.3278	0.1425
Ti	4i	0.8516	0	0.3278	0.8575
O	4i	0.2967	0	0.3483	1
O	4i	0.0414	0	0.3283	1
O	4i	0.6607	0	0.0408	1
O	4i	0.6560	0	0.3004	1

**Table 2** Relative molar quantities of reactants used in preparation of samples

	Ba(CH <sub>2</sub> CO <sub>2</sub> ) <sub>2</sub>	CsNO <sub>3</sub>	Mg(NO <sub>3</sub> ) <sub>2</sub> · 6H <sub>2</sub> O	Al(NO <sub>3</sub> ) <sub>3</sub> · 9H <sub>2</sub> O	Ti[OCH(CH <sub>3</sub> ) <sub>2</sub> ] <sub>4</sub>
	1.2	0.0	1.2 (0.1)		6.8 (0.5)
	1.1	0.1	1.15 (0.1)		6.85 (0.5)
	0.95	0.25	1.075 (0.1)		6.925 (0.5)
	1.2	0.0		2.4 (0.1)	5.6 (0.5)
Figures in brackets indicate excess added to ensure minimum Ti <sup>3+</sup> formation	1.1	0.1		2.3 (0.1)	5.7 (0.5)
	0.95	0.25		2.15 (0.1)	5.85 (0.5)

framework, i.e., it has not currently been possible to determine if there is any superstructure present.

If both of these observations are coupled it can be seen that there is a possibility of some periodicity, e.g., in the system Ba<sub>1.2</sub>Mg<sub>1.2</sub>Ti<sub>6.8</sub>O<sub>16</sub> it is possible to describe a supercell of 5 unit-cells [5]. In many hollandites is incommensurate with respect to the underlying lattice. The effect of adding Cs to a Ba-based hollandite has been studied before [8, 9], however, in the present study we have combined two techniques, neutron diffraction and NMR, which are complementary in nature to provide information on both the long and short range structure in these materials. Because the scattering power of an atom for neutrons has a different dependence on atomic number than with X-rays, neutron diffraction has particular advantages in the study of this system. Cs<sup>+</sup> and Ba<sup>2+</sup>, are iso-electronic, as are Mg<sup>2+</sup> and Al<sup>3+</sup>, thus X-ray diffraction would find it difficult to distinguish between these two pairs of species, whereas they have measurable differences in their neutron scattering lengths ( $b_{\text{Cs}} = 5.42$  fm;  $b_{\text{Ba}} = 5.07$  fm;  $b_{\text{Mg}} = 5.37$  fm;  $b_{\text{Al}} = 3.45$  fm). A second advantage in using neutron diffraction in these systems results from the negative scattering length of Ti ( $b_{\text{Ti}} = -3.44$  fm), which allows for a greater contrast between Al/Ti and Mg/Ti than would be seen with X-rays.

Nuclear magnetic resonance (NMR) is a technique that is element specific and provides information about the local structure in a system. It can be used to study many elements of which the two used here are outlined below:

- i) <sup>133</sup>Cs is a spin  $I = 7/2$  nucleus with 100% natural abundance and a reasonable Larmor frequency ( $\nu_0 = 52.4$  MHz at 9.4 T). Although, <sup>133</sup>Cs is a quadrupolar nucleus, it possesses a very small quadrupolar moment and spectra are generally subject only to a first-order quadrupolar interaction. The non-radioactive <sup>133</sup>Cs nucleus allows directly the investigation of the local environment and dynamic behaviour of Cs nuclei within ceramic wastefoms.
- ii) <sup>27</sup>Al is a spin  $I = 5/2$  nucleus with 100% natural abundance and a high Larmor frequency ( $\nu_0 = 104.3$  MHz at 9.4 T). The quadrupole moment of <sup>27</sup>Al is much larger than <sup>133</sup>Cs and spectra are often affected by a second-order quadrupolar interaction.

## Experimental

### Sample preparation using hot isostatic pressing

Stoichiometric amounts, sufficient to prepare ~200 g of ceramic product, shown in Table 2, of barium acetate (Aldrich, 99.5%), caesium nitrate (Aldrich, 99.99%), aluminium nitrate (Aldrich, 99.5%), and magnesium nitrate (Aldrich, 99.5%) were dissolved in 250–300 mL of deionised water. To the resultant solution a stoichiometric amount of titanium isopropoxide (Aldrich, 98+%) in acetone was added, total volume ~400 mL. A small excess of Mg/Al (0.1 M) and Ti (0.5 M) was added to prevent the formation of Ti<sup>3+</sup>. The resultant flocculant mixture was then homogenised, and stirred while heating until dryness.

Once the mixtures were dried, they were ground in a ball mill until a fine powder was formed. Once formed this powder was then hot isostatically pressed (HIP) at 200 MPa and 1300 °C for 2 h, in a nickel can. Reaction with the can was not expected and the material for subsequent analysis was taken from the middle of the can.

### Elemental analysis using scanning electron microscopy

The samples were checked for purity using a JEOL 6400 SEM operated at 15 kV. Microanalyses were obtained using a Noran Voyager energy dispersive spectrometer (EDX) attached to this microscope. The instrument was operated in standardless mode; however, the sensitivity factors were calibrated for semi-quantitative analysis using a range of synthetic and natural standard materials. Spectra were usually acquired for 500 seconds and reduced to weight percent oxides using a digital top hat filter to suppress the background, a library of reference spectra for multiple least squares peak fitting and full matrix (ZAF) corrections.

### Neutron diffraction

Time-of-flight powder neutron diffraction data were collected using the POLARIS diffractometer at the UK pulsed spallation neutron source ISIS, Rutherford Appleton Laboratory [10, 11]. For each composition studied, between

1 g and 10 g of powdered sample were loaded into a thin-walled, cylindrical vanadium sample can and diffraction data collected for between 185 and 1500  $\mu\text{Ah}$  (equivalent to  $\sim 1\text{--}8$  h neutron beamtime), depending on sample quantity. Summed and normalised data collected in the three available detector banks (A, C, and E) over the time-of-flight range  $\sim 2000\text{--}19,995$   $\mu\text{s}$  (corresponding to a  $d$ -spacing range of  $\sim 0.33\text{--}3.2$   $\text{\AA}$ ) were analysed by the Rietveld Method using the GSAS suite of software [12] with the EXPGUI toolkit [13].

Two structural models, based on hollandites with different symmetries, were refined:

- i) Aluminium and tetragonal magnesium samples—space group  $I4/m$  previously published by Cheary [6].
- ii) The Ba–Mg–Ti–O sample was refined using a modified form of Fanchon's sub-cell structure [5]. The space group setting was changed from  $I12/m1$  to  $I112/m$ , simply by a transformation of axes, allowing comparison of the effect of Cs to be easily contrasted with  $I4/m$ .

In all refinements, however, the remaining sets of parameters refined were identical. A Chebyshev background function was used in all refinements. In each refinement the positional and thermal displacement parameters for those Ba/Cs, Ti/Al and Ti/Mg atom pairs sharing the same crystallographic sites were constrained to be equal. The values for fractional occupancy were constrained to be equal to those determined by AEM analysis. The only exception to this constraint was the Ba–Mg–Ti–O hollandite which had mixing across two sites for Ti and Mg, the occupancies of these two sites were refined with a compositional constraint, of Mg+Ti summing to the total present in the lattice. If after refinement it was found that there was an overall positive charge on the system, using a Ti charge of +4, it was assumed that a proportion of the  $\text{Ti}^{4+}$  has reduced to  $\text{Ti}^{3+}$ . Since the samples once processed were found to be a pale blue, possibly indicative of small amounts of  $\text{Ti}^{3+}$ , this is a reasonable assumption.

#### Nuclear magnetic resonance

$^{133}\text{Cs}$  NMR spectra were acquired using a Varian Infinity Plus spectrometer, equipped with a 11.7 T magnet and operating at a Larmor frequency ( $\nu_0$ ) of 65.6 MHz for  $^{133}\text{Cs}$ . Samples were packed into 7.5-mm diameter  $\text{ZrO}_2$  rotors and rotated at a speed of  $\sim 6$  kHz. Spectra are referenced to 1 M CsCl (aq) via a secondary reference of CsCl (s) at 223.3 ppm [14]. Typically, pulse durations of  $\sim 2$   $\mu\text{s}$  ( $\pi/4$ ) were employed with recycle intervals between 2 and 5 s. Spectra with longer relaxation intervals of  $\sim 60$  s were not significantly different to those obtained with shorter recycle intervals.

$^{27}\text{Al}$  NMR spectra were acquired using a Chemagnetics Infinity spectrometer equipped with a 9.4 T magnet at a  $^{27}\text{Al}$  Larmor frequency of 104.3 MHz. Samples were packed into 4-mm diameter  $\text{ZrO}_2$  rotors and rotated at a speed of  $\sim 12$  kHz. Spectra are referenced to 1 M  $\text{Al}(\text{NO}_3)_3$  (aq), with typical recycle intervals of 2 s. Two-dimensional triple-quantum  $^{27}\text{Al}$  MAS NMR spectra were recorded using a z-filtered pulse sequence [15], resulting in amplitude-modulated data sets. A two-dimensional hypercomplex Fourier transform then yields pure-phase lineshapes. Sign discrimination was achieved through the use of the States–Haberkorn–Ruben method [16]. The radiofrequency fieldstrength applied for the first two pulses (those which excite and convert the triple-quantum coherence) was  $\nu_1 \approx 120$  kHz, whilst the third (central-transition selective) pulse was applied with a much lower radiofrequency fieldstrength,  $\nu_1 \approx 20$  kHz. Isotropic projections were obtained through the use of a frequency-domain shearing transformation with linear interpolation [17].

#### Results and discussion

##### Analytical electron microscopy

The numerical results from the AEM are shown in Table 3. The results show that the predominant hollandite phase varies from the intended composition. This is primarily due to the excess of  $\text{TiO}_2$  and  $\text{MgO}/\text{Al}_2\text{O}_3$  which were added to minimize any  $\text{Ti}^{3+}$  formation. In both sets of samples a  $\text{TiO}_2$  (rutile) impurity was found, while in the Al-containing samples  $\text{Al}_2\text{O}_3$  (corundum) was also found.

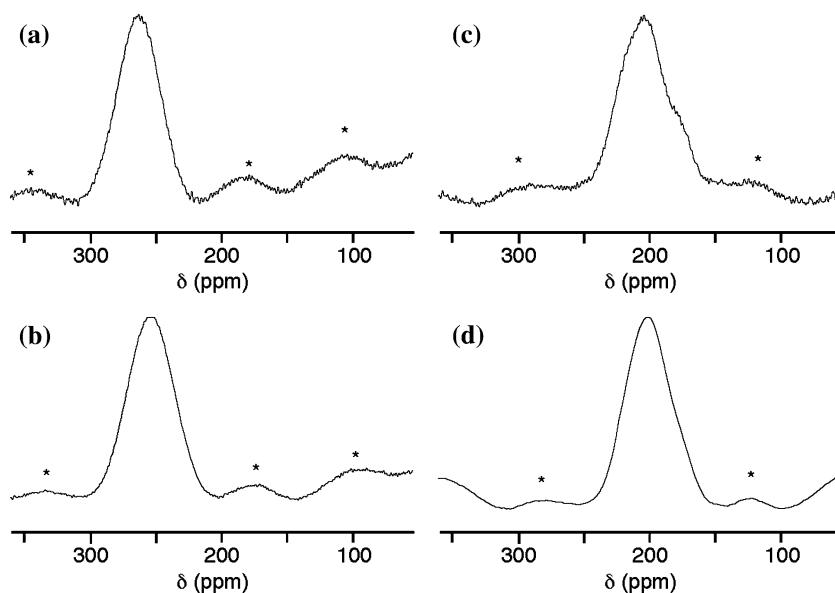
##### $^{133}\text{Cs}$ MAS NMR

Figure 2 shows  $^{133}\text{Cs}$  (65.6 MHz) MAS NMR spectra of Al-containing and Mg-containing hollandites, prepared by HIP, with varying amounts of Cs substitution. For the Al-containing hollandites in Fig. 2(a, b), an intense single peak is observed resulting from the central transition, and a series of spinning sidebands from the satellite transitions. Although the quadrupole moment ( $eQ$ ) of  $^{133}\text{Cs}$  is relatively small [18], the satellite transitions are still significantly broadened over many kHz and split into sidebands under MAS. The single resonance arises from Cs within the channels of the hollandite structure, and as the Cs substitution is increased a small shift in the frequency of the resonance is observed, from 262 ppm to 254 ppm. This value is similar to that observed previously in the literature for an Al-containing hollandite, with the small difference in chemical shift probably reflecting the small difference in chemical composition [19]. In both cases, the peak appears reasonably broad, with a full-width at half-height of around

**Table 3** Scanning electron microscopy elemental analysis results, results shown as molar units converted from weight percent as oxides

Element	Cs	Error	Ba	Error	Sum	
Synthesised composition						
Ba <sub>1.2</sub> Al <sub>2.4</sub> Ti <sub>5.6</sub> O <sub>16</sub>	0.007	0.007	1.181	0.013	1.181	
Ba <sub>1.1</sub> Cs <sub>0.1</sub> Al <sub>2.3</sub> Ti <sub>5.7</sub> O <sub>16</sub>	0.168	0.011	1.034	0.071	1.202	
Ba <sub>0.95</sub> Cs <sub>0.25</sub> Al <sub>2.15</sub> Ti <sub>5.85</sub> O <sub>16</sub>	0.304	0.045	0.922	0.162	1.231	
Ba <sub>1.2</sub> Mg <sub>1.2</sub> Ti <sub>6.8</sub> O <sub>16</sub>	0.007	0.008	1.095	0.038	1.095	
Ba <sub>1.1</sub> Cs <sub>0.1</sub> Mg <sub>1.15</sub> Ti <sub>6.85</sub> O <sub>16</sub>	0.169	0.015	0.940	0.065	1.117	
Ba <sub>0.95</sub> Cs <sub>0.25</sub> Mg <sub>1.075</sub> Ti <sub>6.925</sub> O <sub>16</sub>	0.315	0.011	0.862	0.039	1.177	
Element	Ti	Error	Al	Error	Mg	Error
Synthesised composition						
Ba <sub>1.2</sub> Al <sub>2.4</sub> Ti <sub>5.6</sub> O <sub>16</sub>	6.087	0.004	1.903	0.012		
Ba <sub>1.1</sub> Cs <sub>0.1</sub> Al <sub>2.3</sub> Ti <sub>5.7</sub> O <sub>16</sub>	6.209	0.007	1.771	0.005		
Ba <sub>0.95</sub> Cs <sub>0.25</sub> Al <sub>2.15</sub> Ti <sub>5.85</sub> O <sub>16</sub>	6.226	0.077	1.753	0.079		
Ba <sub>1.2</sub> Mg <sub>1.2</sub> Ti <sub>6.8</sub> O <sub>16</sub>	7.074	0.019			0.907	0.024
Ba <sub>1.1</sub> Cs <sub>0.1</sub> Mg <sub>1.15</sub> Ti <sub>6.85</sub> O <sub>16</sub>	7.128	0.016			0.860	0.015
Ba <sub>0.95</sub> Cs <sub>0.25</sub> Mg <sub>1.075</sub> Ti <sub>6.925</sub> O <sub>16</sub>	7.179	0.018			0.809	0.009

**Fig. 2** Normalised <sup>133</sup>Cs (65.6 MHz) MAS NMR spectra of hollandite phases with nominal composition (a) Ba<sub>1.1</sub>Cs<sub>0.1</sub>Al<sub>2.16</sub>Ti<sub>5.84</sub>O<sub>16</sub>, (b) Ba<sub>0.95</sub>Cs<sub>0.25</sub>Al<sub>2.048</sub>Ti<sub>5.952</sub>O<sub>16</sub>, (c) Ba<sub>1.1</sub>Cs<sub>0.1</sub>Mg<sub>1.124</sub>Ti<sub>6.876</sub>O<sub>16</sub> and (d) Ba<sub>0.95</sub>Cs<sub>0.25</sub>Mg<sub>1.15</sub>Ti<sub>6.85</sub>O<sub>16</sub>. All spectra are the result of averaging 4000 transients with a recycle interval of 2 s. The MAS rate was 6 kHz. Spectra are referenced to 1 M CsCl (aq), and are shown plotted against ppm (δ). Spinning sidebands are indicated by \*



2.5 kHz. This results from a distribution of <sup>133</sup>Cs chemical shifts (on the order of ±16 ppm), reflecting the distribution of Cs local environments within the structure. This may be due to a disorder in the position of Cs within the channels or to a disorder in the framework structure.

The <sup>133</sup>Cs MAS NMR spectra of the Mg-containing hollandites are shown in Fig. 2(c, d). Although a broad resonance is again observed, the substitution of Al for Mg in the framework results in a significant shift (of around –50 ppm) of the peak, reflecting the difference in the extended coordination environment of Cs. As was observed for the Al-containing samples, the chemical shift of the resonance decreases with increasing Cs substitution, although the change is smaller in this case, i.e., from 205 to

201 ppm. Although both resonances are again reasonably broad, both exhibit a distinct shoulder (around 179 ppm) indicative of a second distinct Cs environment. This is particularly obvious for the case of the lower Cs substitution in Fig. 2c. One possible explanation may be the presence of differing next-nearest neighbour coordinating atoms, i.e., Cs–O–Mg and Cs–O–Ti linkages. It should be noted that the presence of a second peak within the broad resonance found in the Al-containing hollandites cannot be discounted.

Previous work has shown that the presence of any paramagnetic Ti<sup>3+</sup> within the hollandite framework leads to a considerable shift of the Cs resonance (for example to around 400 ppm in a Al-containing hollandite and

~600 ppm in a Mg-containing hollandite [20]) and a significant spectral broadening. None of the spectra in Fig. 2 display any evidence of  $\text{Ti}^{3+}$  within the framework structure. In both Al- and Mg-containing materials, the  $^{133}\text{Cs}$   $T_1$  relaxation times are relatively long, between >30 s. This reflects the small quadrupolar interaction (i.e., little quadrupolar relaxation) and lack of any significant motion of the Cs along the channels at room temperature. In addition, the long relaxation times reinforce the lack of significant amounts of (paramagnetic)  $\text{Ti}^{3+}$  within the framework.

### $^{27}\text{Al}$ MAS NMR

As Al is a spin  $I = 5/2$  nucleus it possesses a quadrupole moment ( $eQ$ ) which can interact with the electric field gradient ( $eq$ ) present at the nucleus, resulting in a broadening of the spectrum. This quadrupolar interaction can be parametrised by its magnitude  $C_Q = e^2qQ/h$  and asymmetry,  $\eta$ , defined such that  $0 < \eta < 1$  [21]. Although the quadrupolar interaction may be large, broadening spectra over kHz or MHz, the central ( $|+1/2\rangle \leftrightarrow |-1/2\rangle$ ) transition is unaffected by the quadrupolar interaction to first order and remains sharp, as was observed in the  $^{133}\text{Cs}$  spectra in Fig. 2. However, for  $^{27}\text{Al}$ , unlike  $^{133}\text{Cs}$ , the quadrupolar interaction is often very large and a second-order approximation must be considered to describe its effect upon the spectrum. The central transition is affected by the quadrupolar interaction to second-order and exhibits an anisotropically broadened powder-pattern lineshape. Although MAS can narrow the line it cannot remove second-order quadrupolar broadening fully and the central transition remains broadened, with the appearance of the lineshape dependant upon  $C_Q$  and  $\eta^{21}$ . However, for disordered solids the distribution of local environments produces, in addition to a distribution of chemical shifts, a distribution of quadrupolar parameters. In this case the central-transition is further broadened and often displays an asymmetric lineshape with a “tail” to low frequency [22, 23].

Figure 3 shows  $^{27}\text{Al}$  (104.3 MHz) MAS NMR spectra of spectra of Al-containing hollandites, prepared by HIP, with varying amounts of Cs substitution. In Fig. 3a, the spectrum of a hollandite with no Cs substitution, a broad, slightly asymmetric lineshape is observed with an observed chemical shift,  $\delta$ , of approximately -6 ppm. This is typical of Al in an octahedrally coordinated environment [22]. The lack of any features characteristic of second-order quadrupolar broadening suggest that a distribution of environments is present (and hence a distribution of chemical shift and quadrupolar parameters) as a result of disorder. This disorder cannot result from the incorporation of Cs within the structure and so must result from that present in the framework. Although asymmetric, the lack of a long tail to

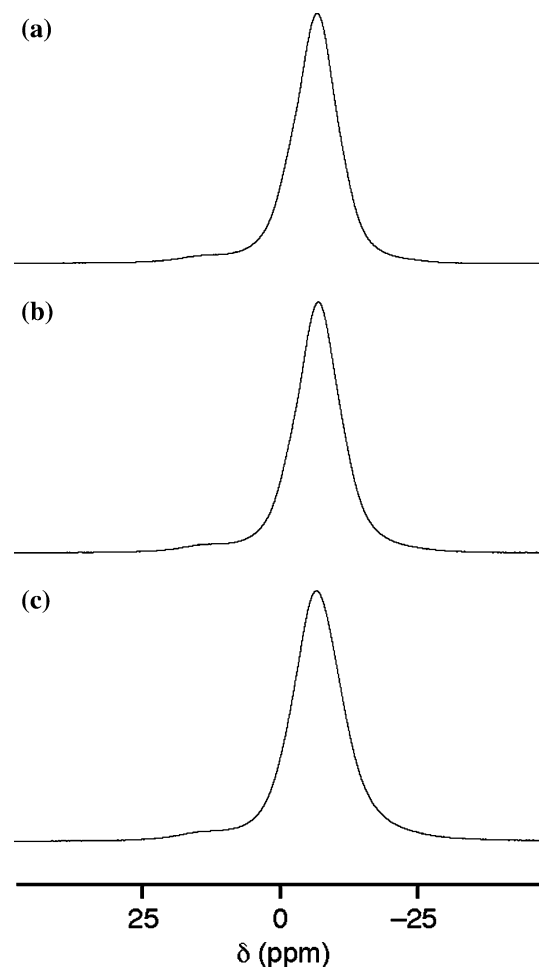


**Fig. 3**  $^{27}\text{Al}$  (104.3 MHz) MAS NMR spectra of hollandite phases with nominal composition (a)  $\text{Ba}_{1.2}\text{Al}_{2.136}\text{Ti}_{5.864}\text{O}_{16}$ , (b)  $\text{Ba}_{1.1}\text{Cs}_{0.1}\text{Al}_{2.16}\text{Ti}_{5.84}\text{O}_{16}$  and (c)  $\text{Ba}_{0.95}\text{Cs}_{0.25}\text{Al}_{2.048}\text{Ti}_{5.952}\text{O}_{16}$ . All spectra are the result of averaging 2000 transients with a recycle interval of 2 s. The MAS rate was 11 kHz. Spectra are referenced to 1 M  $\text{Al}(\text{NO}_3)_3$  (aq), and are shown plotted against ppm ( $\delta$ )

low frequency suggests that the quadrupolar interaction (or its distribution) are fairly small. As the Cs content of the hollandite is increased little change is observed in the spectrum. The width of the resonance increases slightly (as a result of the increased disorder), shifting the centre-of-gravity very slightly to lower frequency.

The presence of second-order quadrupolar broadening in the central-transition MAS NMR spectrum of half-integer quadrupolar nucleus decreases the resolution of distinct species and hinders the extraction of useful information. One approach for the removal of this broadening is the multiple-quantum MAS (MQMAS) experiment [24]. This is a two-dimensional experiment involving the correlation of a “forbidden” multiple-quantum transition (usually triple-quantum) and the central transition in a two-dimensional experiment under MAS conditions. This removes all anisotropic broadening but retains isotropic (both chemical

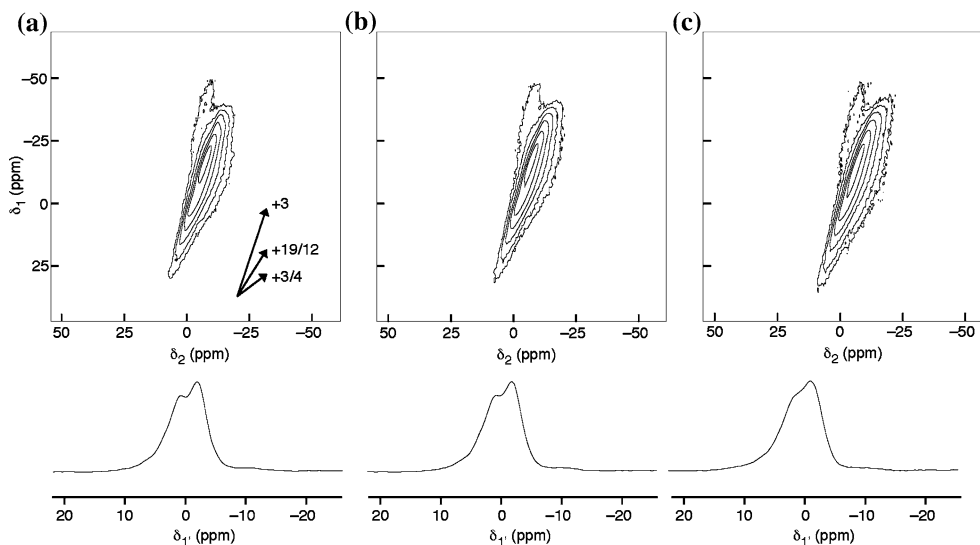
and quadrupolar) shifts [24, 25]. For a well-crystalline solid this allows the acquisition of a high-resolution or “isotropic” spectrum consisting of sharp, narrow resonances. High-resolution spectra of disordered solids cannot be obtained in the same way as these lineshapes are also broadened by distributions of the isotropic parameters. This is equivalent to having many ridges with very slightly differing parameters very closely spaced in the two-dimensional spectrum. However MQMAS spectra of disordered solids do offer an increase in resolution and may, therefore, be able to distinguish whether the broadened disordered lineshapes result from the overlap of more than one different Al site [22, 23].

Figure 4 shows two-dimensional  $^{27}\text{Al}$  (104.3 MHz) triple-quantum MAS NMR spectra of hollandite phases with varying Cs content, prepared by HIP. Spectra were recorded using a z-filtered pulse sequence [15] and the States–Haberkm–Ruben method [16] was used to restore sign discrimination. A broad resonance is observed which, on closer inspection, may be seen to comprise of two closely spaced resonances, indicating two distinct Al species. This is more apparent in the isotropic projections also shown in Fig. 4, obtained from the two-dimensional spectrum after a frequency-domain shearing transformation. Although substantial broadening is observed along an axis of +19/12 (that expected for crystalline materials), broadening along other axes do confirm the presence of distributions of both chemical shift (along +3) and quadrupolar parameters (along +3/4) [23, 26]. It should be

noted, however that the distribution of the latter appears reasonably small.

For crystalline materials, the position of the centre-of-gravity of a two-dimensional lineshape in an MQMAS spectrum provides information on the isotropic chemical shift,  $\delta_{\text{CS}}$ , (i.e., not the observed MAS shift) and the quadrupolar product  $P_{\text{Q}}$ , (given by  $C_{\text{Q}}(1 + \eta^2/3)^{1/2}$ ). For disordered or amorphous materials only average values,  $\langle\delta_{\text{CS}}\rangle$  and  $\langle P_{\text{Q}}\rangle$ , can be obtained owing to the distributions present in these parameters [23]. For the spectrum shown in Fig. 4(a), values of  $\langle\delta_{\text{CS}}\rangle = -4.7 \pm 1$  ppm and  $\langle P_{\text{Q}}\rangle = 2.2 \pm 0.4$  MHz and  $\langle\delta_{\text{CS}}\rangle = -1 \pm 1$  ppm and  $\langle P_{\text{Q}}\rangle = 3.1 \pm 0.4$  MHz are obtained for the two components in order of increasing  $\delta_1$  shift. Both chemical shifts are typical of octahedrally coordinated Al and both quadrupolar coupling constants are relatively small, indicating a reasonably symmetric local environment. It should be noted that the substantial overlap of the two species in the two-dimensional spectrum does hinder the determination of the exact position of the centre-of-gravity in each case and the values quoted above should be treated with caution.

Little difference in the spectrum is observed as the Cs content increases. The width of both resonances increases slightly as a result of increasing disorder and the resolution between the two in the isotropic projection is therefore decreased. The centre-of-gravity of the two peaks remains very similar giving similar average values of  $P_{\text{Q}}$  and  $\delta_{\text{CS}}$ , but the distribution of the parameters present appears to increase slightly.



**Fig. 4** Two-dimensional  $^{27}\text{Al}$  (104.3 MHz) triple-quantum MAS NMR spectra and corresponding isotropic projections of hollandite phases with nominal composition (a)  $\text{Ba}_{1.2}\text{Al}_{2.136}\text{Ti}_{5.864}\text{O}_{16}$ , (b)  $\text{Ba}_{1.1}\text{Cs}_{0.1}\text{Al}_{2.16}\text{Ti}_{5.84}\text{O}_{16}$  and (c)  $\text{Ba}_{0.95}\text{Cs}_{0.25}\text{Al}_{2.048}\text{Ti}_{5.952}\text{O}_{16}$ . Spectra were recorded using a z-filtered pulse sequence and using the States–Haberkm–Ruben method to restore sign discrimination.

In all cases, 240 transients were averaged with a recycle interval of 2 s for each of 80  $t_1$  increments of 50  $\mu\text{s}$ . The MAS rate was 11 kHz. Spectra are referenced to 1 M  $\text{Al}(\text{NO}_3)_3$  (aq). Isotropic projections were obtained through the use of a frequency-domain shearing transformation with linear interpolation

## Neutron diffraction

### Aluminium-containing samples

In these samples the structure refinement results (Fig. 5), show that as the concentration of Cs increases there is a change in the unit-cell parameters (Table 4 and Fig. 6). This change is to be expected, the ionic radius of  $\text{Cs}^+$  (1.74 Å) is larger than that of  $\text{Ba}^{2+}$  (1.42 Å). Therefore, any direct replacement of  $\text{Cs}^+$  for  $\text{Ba}^{2+}$  should result in a proportional change. It should be added that although there is a change in the  $\text{Al}^{3+}/\text{Ti}^{4+}$  ratio, with an average ionic-radius increase, the change here is linked directly with the addition of  $\text{Cs}^+$  i.e.,  $\text{Ba}^{2+} \rightarrow \text{Cs}^+$  and  $\text{Al}^{3+} \rightarrow \text{Ti}^{4+}$ . Since  $\text{Ti}^{4+}$  (0.605 Å) [27, 28] is larger than  $\text{Al}^{3+}$  (0.535 Å) an increase in unit-cell volume is expected.

The variation in the unit-cell  $a$ -parameter is found to be linear, while that in the  $c$ -parameter is not. One possible explanation for this is that since the  $a$ -parameter is directly related to the diameter of the channels and with no overall change in the occupancy of tunnel sites (total A site content remains constant at 1.2 atoms per formula unit) the change

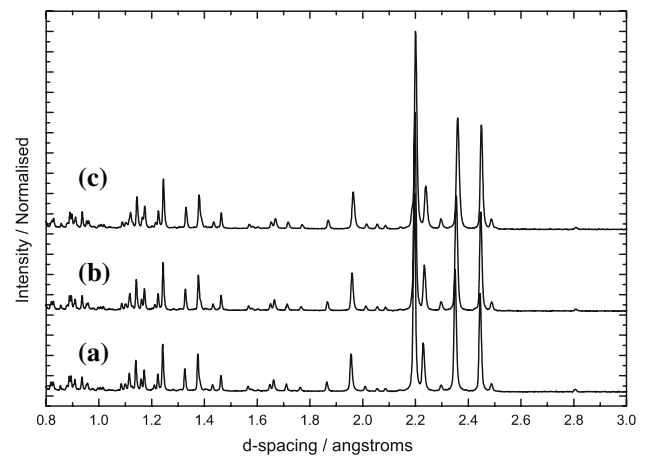


**Fig. 5** Normalised neutron diffraction patterns collected in the Polaris backscattering detector bank ( $\langle 2\theta \rangle = 145^\circ$ ) from the Al-containing hollandite samples

in the  $a$ -parameter reflects only a change in the average radius of the A cations. The variation in the  $c$ -parameter is more complex as this is determined not only by the

**Table 4** Results from Rietveld profile refinement for aluminium-containing hollandites

Atom	Wyckoff	X	Y	Z	$U_{\text{ISO}}$	Frac
$\text{Ba}_{1.181}\text{Al}_{1.903}\text{Ti}_{6.087}\text{O}_{16}$			$a = 9.96476(10)$	$b = 9.96476(10)$	$c = 2.92210(3)$	
		SPGR	I4/m	wRp = 0.0304		
Ba	4e	0	0	0.9023(11)	0.0270(9)	0.2952
Ti	8h	0.1465(2)	0.6680(2)	0	0.0251(3)	0.7609
Al	8h	0.1465(2)	0.6680(2)	0	0.0251(3)	0.2379
O	8h	0.3470 (5)	0.7020(4)	0	0.0063(2)	1.0
O	8h	0.3334(5)	0.9588(4)	0	0.0075(2)	1.0
$\text{Ba}_{1.034}\text{Cs}_{0.168}\text{Al}_{1.771}\text{Ti}_{6.209}\text{O}_{16}$			$a = 9.98353(10)$	$b = 9.98353(10)$	$c = 2.92388(4)$	
		SPGR	I4/m	wRp = 0.0312		
Ba	4e	0	0	0.9089(11)	0.0245(8)	0.2585
Cs	4e	0	0	0.9089(11)	0.0245(8)	0.042
Ti	8h	0.1476(2)	0.6683(9)	0	0.0244(3)	0.7761
Al	8h	0.1476(2)	0.6683(9)	0	0.0244(3)	0.2214
O	8h	0.3463(5)	0.7022(4)	0	0.0054(1)	1.0
O	8h	0.3345(2)	0.9584(4)	0	0.0088(4)	1.0
$\text{Ba}_{0.922}\text{Cs}_{0.304}\text{Al}_{1.753}\text{Ti}_{6.226}\text{O}_{16}$			$a = 10.0068(8)$	$b = 10.0068(8)$	$c = 2.9247(4)$	
		SPGR	I4/m	wRp = 0.0336		
Ba	4e	0	0	0.9132(13)	0.0268(9)	0.2305
Cs	4e	0	0	0.9132(13)	0.0268(9)	0.0760
Ti	8h	0.1487(3)	0.6677(4)	0	0.0213(3)	0.744(6)
Al	8h	0.1487(3)	0.6677(4)	0	0.0213(3)	0.256(6)
O	8h	0.3460(6)	0.7029(7)	0	0.0059(4)	1.0
O	8h	0.3346(5)	0.9585(4)	0	0.0094(5)	1.0

Figures in brackets are the esds on the least significant figure(s), as calculated by GSAS. Unit cell dimensions are in Angstroms, wRp is the average value for all 3 detector banks given by GSAS during refinement. The additional phases of  $\text{TiO}_2$  (rutile) and  $\text{Al}_2\text{O}_3$  (corundum) have been omitted from the data above

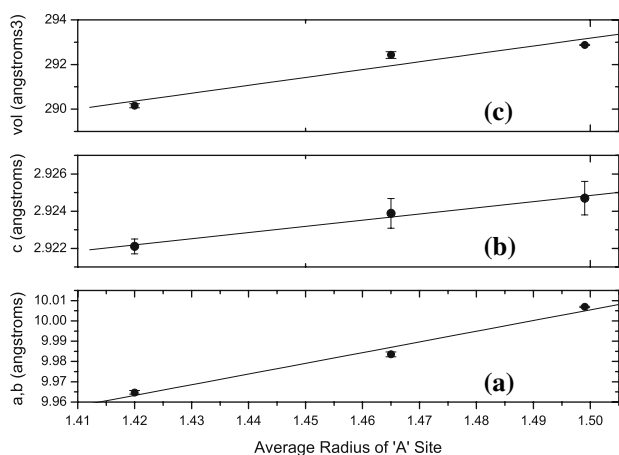


**Fig. 6** Unit cell parameters for Al-containing hollandite samples shown as a function of Ba composition, plot (a) shows the  $a,b$ -parameter, (b) the  $c$ -parameter, (c) the volume; error bars are those given by GSAS from the refinements

constituent atoms, but also the degree of ordering across the positions available and the partial occupancies observed.

There is a discrepancy between the Al environments indicated by the NMR and neutron diffraction experiments. The NMR spectra provide evidence for two Al species in the crystal, whilst there is no direct evidence of this in the structure refined from the neutron diffraction data. The most likely explanation is to the presence of both edge-sharing and corner-sharing octahedra. One Al species is Al–O–Al/Ti in the corner-sharing octahedra, while the other is Al–O–O–Al/Ti, in the edge-sharing octahedra. These two slightly different positions result in two Al–Al/Ti distances which are  $\sim 3.0$  Å for edge sharing and  $\sim 3.4$  Å for corner sharing. Such a difference is geometric in nature, and arises from one crystal site, as a result MAS NMR sees slightly different geometry, and local composition once the disorder present in the B-site is accounted for, as it is more sensitive to local structure, while neutron diffraction sees only the one. The presence of two peaks in the Al spectrum is not a result of Cs/Ba disorder in the tunnels, as two peaks are also observed in  $\text{Ba}_{1.2}\text{Al}_{2.136}\text{Ti}_{5.864}\text{O}_{16}$  (Fig. 7).

#### Magnesium-containing samples

The results obtained by the Rietveld refinement show a substantial change as  $\text{Cs}^+$  is added to the structure, (Table 5 and Figs. 8, 9). Upon addition of  $\text{Cs}^+$  there is a change from monoclinic to tetragonal symmetry. Such an observation has been reported by Cheary as being due to “the large Cs ions prevent the tunnel walls collapsing onto the tunnel ions” [8].

The  $\text{Cs}^+$  containing samples do show a change in cell volume as the Cs-content is increased, but as there are only

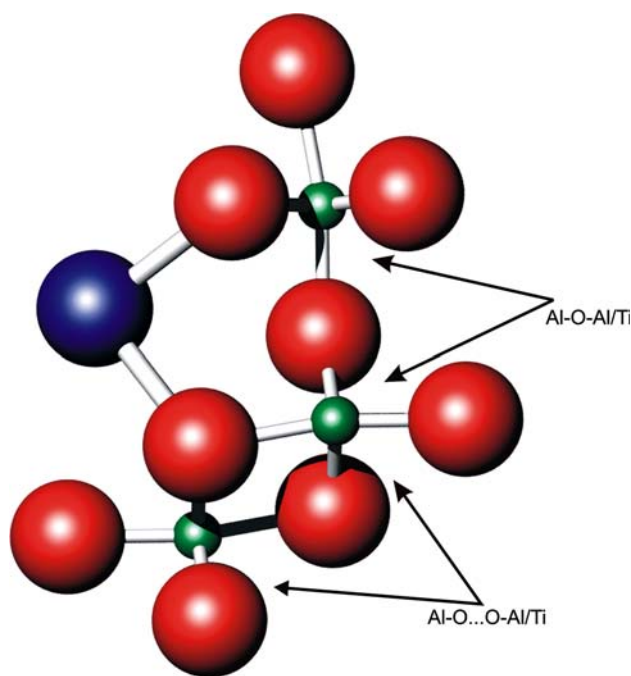


**Fig. 7** Portion of hollandite structure showing the two types of Al–O bonds in the corner and edge sharing octahedral, large black spheres are the A cations, small black spheres are the B cations, and large grey spheres are the O anions

two samples there are insufficient points to be sure of a trend. There will be a similar effect of radius change upon  $\text{Cs}^+$  for  $\text{Ba}^{2+}$  replacement, but in these systems there is a counter effect of  $\text{Mg}^{2+}$  ( $0.72$  Å) being replaced by the smaller  $\text{Ti}^{4+}$  ( $0.605$  Å). Any increase in tunnel size may be offset by a change in wall thickness.

The degree of shearing from the monoclinic system to the tetragonal system is  $\sim 0.5^\circ$ , a very small change that has little effect on the volume of the unit cell. This observation demonstrates the close relationship between the monoclinic and tetragonal hollandite structures.

The diffraction data for the  $\text{Ba}_{1.095}\text{Mg}_{0.907}\text{Ti}_{7.074}\text{O}_{16}$  system showed no evidence of a super-cell, observed by Fanchon et al. [5] in  $\text{Ba}_{1.2}\text{Mg}_{1.2}\text{Ti}_{6.8}\text{O}_{16}$ . This could be due to many reasons; the most likely is that as these samples were measured as fine powders sample broadening may have masked the small degree of monoclinic splitting. The values do agree however, with the values reported for the sub-cell.

#### Comparison of tetragonal hollandites

A statistical analysis of the  $a$  and  $c$  cell parameters for a set of 27 synthetic and natural tetragonal hollandite samples from the literature has been undertaken. The data used for this analysis were obtained from Sinclair et al. [29]; Cheary [6, 8, 30]; Vogt et al. [31]; Watanabe et al. [32];

**Table 5** Results from Rietveld profile refinement for magnesium-containing hollandites

Atom	Wyckoff	X	Y	Z	U <sub>ISO</sub>	Frac
Ba <sub>1.095</sub> Mg <sub>0.907</sub> Ti <sub>7.074</sub> O <sub>16</sub>			a = 10.1809(2)	b = 10.0158(3)	c = 2.9728(4)	γ = 90.520(2)
		SPGR	I112/m	wRp = 0.0381		
Ba	4g	0	0	0.3509(23)	0.0157(14)	0.1825
Ba	2b	0	0	0.5000	0.0157(14)	0.1825
Ti	4i	0.3499 (3)	0.8294 (3)	0	0.0113(6)	0.897(2)
Mg	4i	0.3499 (3)	0.8294 (3)	0	0.0113(6)	0.101(2)
Ti	4i	0.8287 (3)	0.6549 (5)	0	0.0067 (7)	0.872(2)
Mg	4i	0.8287 (3)	0.6549 (5)	0	0.0067 (7)	0.126(2)
O	4i	0.1557 (5)	0.8004 (1)	0	0.0277 (26)	1
O	4i	0.1610 (7)	0.5406 (4)	0	0.0905 (28)	1
O	4i	0.7964 (6)	0.8489 (7)	0	0.0715 (30)	1
O	4i	0.5416 (8)	0.8266 (8)	0	0.0608 (30)	1
Ba <sub>0.94</sub> Cs <sub>0.169</sub> Mg <sub>0.860</sub> Ti <sub>7.128</sub> O <sub>16</sub>			a = 10.1130 (1)	b = 10.1130 (1)	c = 2.9722 (6)	
		SPGR	I4/m	wRp = 0.0422		
Ba	4e	0	0	0.8985 (15)	0.0168 (11)	0.2350
Cs	4e	0	0	0.8985 (15)	0.0168 (11)	0.0422
Ti	8h	0.1510 (6)	0.6691 (8)	0	0.0140 (6)	0.8910
Mg	8h	0.1510 (6)	0.6691 (8)	0	0.0140 (6)	0.1075
O	8h	0.3452 (8)	0.7023 (7)	0	0.0080(8)	1.0
O	8h	0.3331 (2)	0.9589 (1)	0	0.0079 (2)	1.0
Ba <sub>0.862</sub> Cs <sub>0.315</sub> Mg <sub>0.809</sub> Ti <sub>7.179</sub> O <sub>16</sub>			a = 10.1302(2)	b = 10.1302(2)	c = 2.9710(9)	
		SPGR	I4/m	wRp = 0.0397		
Ba	4e	0	0	0.8927(13)	0.0176 (10)	0.2155
Cs	4e	0	0	0.8927(13)	0.0176 (10)	0.0787
Ti	8h	0.1520(2)	0.6682(4)	0	0.0132 (3)	0.8974
Mg	8h	0.1520(2)	0.6682(4)	0	0.0132 (3)	0.1011
O	8h	0.3452(2)	0.7030(2)	0	0.0079 (8)	1.0
O	8h	0.3337(9)	0.9592(6)	0	0.0093 (2)	1.0

Figures in brackets are the esds on the least significant figure(s), as calculated by GSAS. Unit cell dimensions are in Angstroms, wRp is the average value for all 3 detector banks given by GSAS during refinement. The additional phases of TiO<sub>2</sub> (rutile) has been omitted from the data

Pring et al. [33]; Onoda et al. [34]; Weber and Schultz [35]. We are currently evaluating additional data for future work of this type, including monoclinic hollandite compounds. The analyses involved modelling of published lattice parameters against the mean ionic radii ( $R_A$ ) of the tunnel cations, mean ionic radii ( $R_B$ ) of the octahedral framework cations, tunnel occupancy  $x$ , and the average formal valence states ( $V_A$ ) of the tunnel cations. Although the formal valence state is related to the ionic radius, we tested this parameter as a possible indicator of A-site cation repulsion in the tunnels. Statistical analyses were performed using the multiple regression module of Statistica, wherein the lattice parameters are treated as dependent variables and  $R_A$ ,  $R_B$ ,  $x$ , and  $V_A$  were used as the independent variables. We included an intercept in the models, as is typical for this type of analysis [36, 37]. The best

models were derived using stepwise regression procedures. Results of this analysis gave the following linear equations for the lattice parameters of the tetragonal hollandite structure:

$$a = 0.4331 (R_A) + 4.1725 (R_B) - 0.0995 (x) - 0.0706 (V_A) + 7.1621 (R^2 = 0.994) \quad (1)$$

$$c = -0.0983 (R_A) + 1.8517 (R_B) - 0.0175 (V_A) + 2.0129 (R^2 = 0.888) \quad (2)$$

$$V = 17.8043 (R_A) + 458.3978 (R_B) - 3.9146 (V_A) (R^2 = 0.976) \quad (3)$$

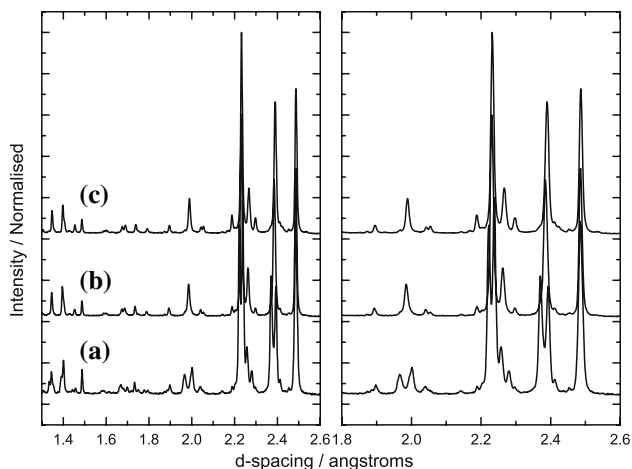


**Fig. 8** Normalised neutron diffraction patterns collected in the Polaris backscattering detector bank ( $\langle 2\theta \rangle = 145^\circ$ ) from the Mg-containing hollandite samples, graph on right is an expanded region showing the change in symmetry

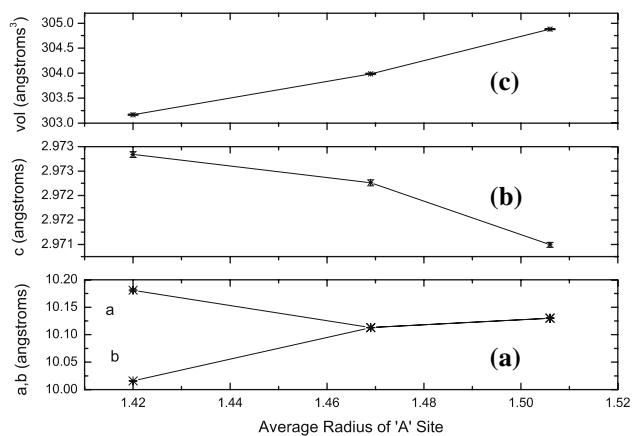


**Fig. 9** Unit cell parameters for Mg-containing hollandite samples shown as a function of Ba composition, plot (a) shows the  $a,b$ -parameter, (b) the  $c$ -parameter, (c) the volume; error bars are those given by GSAS from the refinements

The full statistics are listed in Table 6. Regression coefficients indicate that the  $a$  cell dimension is mainly dependent upon the radius of the B-site cation, by a factor of nearly ten over that of the tunnel cation. The  $a$  cell dimension also has weak, but significant, negative correlations with the tunnel occupancy and valence (see statistics in Table 5). Overall, the dependence of the  $c$  cell dimension on these parameters is much poorer as reflected by the regression statistics, and the effect of tunnel occupancy is not significant based on the Students  $t$ -test. Regression data show that  $c$  is also mainly dependent upon the radius of the B-site cation and has small negative correlations with the tunnel cation radius and valence state. These results demonstrate that the size of the unit cell of tetragonal hollandite is mainly controlled by the radii of the

**Table 6** Results obtained from the statistical analysis of hollandites, the values of  $R^2$  and standard deviation (SD) are those outputted by Statistica

Coefficient	Value	Error	$t$ -Test value
Unit-cell parameter a		$R^2 = 0.994$	SD = 0.008
$R_B$	4.1725	0.1311	31.82
$x$	-0.0175	0.0253	-3.93
$V_A$	-0.0706	0.0107	-6.60
Intercept	7.1621	0.1301	
Unit-Cell Parameter c		$R^2 = 0.888$	SD = 0.011
$R_A$	-0.0983	0.0411	-2.39
$R_B$	1.8517	0.1497	12.37
$V_A$	-0.0175	0.0074	-2.35
Intercept	2.0129	0.1072	
Unit-Cell Volume		$R^2 = 0.976$	SD = 1.446
$R_A$	17.8043	5.4322	3.27
$R_B$	458.3978	19.7802	23.17
$V_A$	-3.9146	0.9817	-3.99
Intercept	3.9416	14.1569	

B-site cations in the tunnel walls. The regression equation for the unit cell volume follows from these observations, but in this case the intercept is not significant.

The use of Eqs. 1 + 2, although empirical in nature, allows a prediction of the unit cell size of hollandites to be made. If these equations are compared with those previously published by Zhang et al., Eqs. 4 + 5, a difference is noticed.

$$a = 5.130(R_O + R_B) - 0.0291Z_B + 0.441\delta_A \quad (4)$$

$$c = \sqrt{2}(R_O + R_B) + 0.0366Z_B + 0.552\delta_B \quad (5)$$

where  $R_O$  and  $R_B$  are the ionic radii of the B-site cations,  $Z_B$  the total charge of the B-site cations,  $\delta_A$  and  $\delta_B$  are determined by the following equations:

$$\begin{aligned} \delta_A &= (R_O + R_B) - \sqrt{2}(R_O + R_B) \\ &\text{if } R_O + R_A \geq \sqrt{2}(R_O + R_B) \\ \delta_A &= 0 \\ &\text{if } R_O + R_A < \sqrt{2}(R_O + R_B) \end{aligned} \quad (6)$$

$$\begin{aligned} \delta_B &= R_B - 0.414R_O \quad \text{if } R_B \geq 0.414R_O \\ \delta_B &= 0 \quad \text{if } R_B < 0.414R_O \end{aligned} \quad (7)$$

If the above equations are used then the obtained results differ from the experimental values with a larger discrepancy, shown in Table 7 with example plot in Fig. 10, than those predicted by Eqs. 1 + 2. One likely explanation is that the generation of Eqs. 1 + 2 used a different basis, in both published structures used and methodology to

**Table 7** Calculated and observed values for tetragonal hollandites using Eqs. 1–6

System	Average Ra/Å	Average Rb/Å	Obs a/Å	New Model a/Å	Zhang Model a/Å	Obs c/Å	New Model c/Å	Zhang Model c/Å
Ba <sub>0.94</sub> Cs <sub>0.169</sub> Mg <sub>0.860</sub> Ti <sub>7.128</sub> O <sub>16</sub>	1.469	0.620	10.113	9.087	10.139	2.972	2.981	3.856
Ba <sub>0.862</sub> Cs <sub>0.304</sub> Mg <sub>0.809</sub> Ti <sub>7.170</sub> O <sub>16</sub>	1.506	0.620	10.130	9.064	10.157	2.971	2.980	3.839
Ba <sub>1.181</sub> Al <sub>1.903</sub> Ti <sub>6.087</sub> O <sub>16</sub>	1.420	0.592	9.9648	9.055	9.984	2.922	2.932	3.836
Ba <sub>1.034</sub> Cs <sub>0.168</sub> Al <sub>1.771</sub> Ti <sub>6.209</sub> O <sub>16</sub>	1.465	0.593	9.9835	9.071	10.012	2.934	2.930	3.840
Ba <sub>0.922</sub> Cs <sub>0.304</sub> Al <sub>1.753</sub> Ti <sub>6.226</sub> O <sub>16</sub>	1.499	0.592	10.007	9.080	10.030	2.925	2.928	3.843

Average values for ionic radii taken from Shannon [28, 29] for atoms in octahedral co-ordination. The radius used for Ti has been averaged from Ti<sup>4+</sup> and Ti<sup>3+</sup> using calculated values to maintain charge neutrality

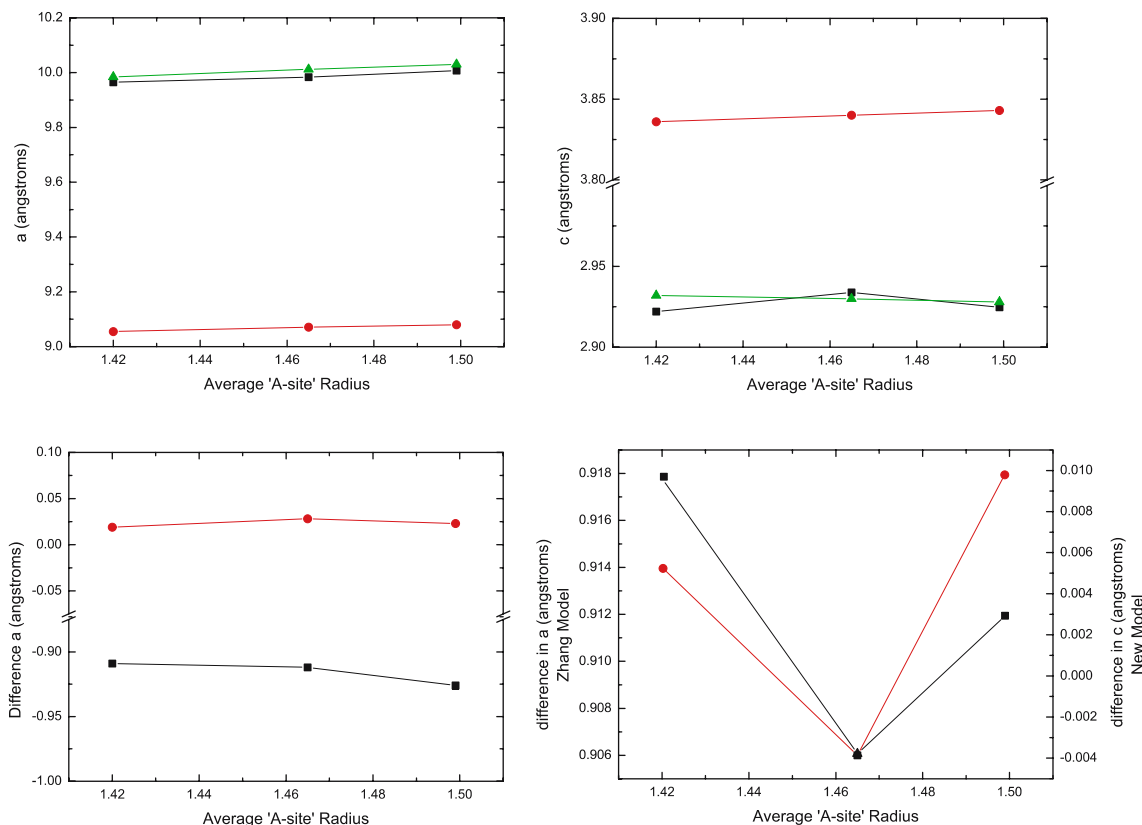


**Fig. 10** Plots of predicted values from the Zhang model and the new model presented here for the Al-based systems, **(a)** *a*-parameter, **(b)** difference between calculated and observed for the *a*-parameter, **(c)** *c*-parameter, and **(d)** the difference between calculated and

observed for the *c*-parameter. In all plots the same markers are used. In **(d)** the scale to the right is that for the new model, while the left is that for the Zhang model. In all plots circles are the Zhang model, squares the new model presented here and the triangles are the recorded data

Eqs. 4 + 5. However, Eqs. 1 + 2 seem to give a better agreement to the recorded data presented here.

## Conclusions

The addition of Cs<sup>+</sup> to hollandite lattices results in the Cs<sup>+</sup> being located in the tunnels, this has been confirmed by both neutron diffraction and <sup>133</sup>Cs MAS NMR. It has been shown that increasing the amount of Cs<sup>+</sup> present has little effect on

its location within the tunnels, and more importantly it does not enter and become part of the tunnel wall structure. The <sup>27</sup>Al NMR data has shown that addition of Cs<sup>+</sup> has little effect on the ordering of Al, and therefore Ti, in the tunnel walls. A statistical algorithm has been found that can describe, with reasonable accuracy, both the *a* and *c* unit-cell parameters in tetragonal hollandites, this can be used to predict the likely unit-cell sizes for new compositions.

**Acknowledgments** The authors wish to acknowledge the help of Dr E.R. Maddrell at British Nuclear Fuels Limited for helpful

discussions, CMI—The Cambridge MIT Institute (KRW) and the EPSRC for funding this work.

## References

1. Carter ML (2004) *Mater Res Bull* 39:1075
2. Ramakrishnan PA, Sugantha M, Varadaraju UV, Nagarajan T (1998) *Mater Lett* 36:137
3. Chu LW, Hsiue GH, Chiang YJ, Liu KS, Lin IN (2004) *J Eur Ceramic Soc* 24:1781
4. Guignot N, Andrault D (2004) *Phys Earth Planet Interiors* 143–144:107
5. Fanchon E, Vicat J, Hodeau JL, Wolfers P, Qui DT, Strobel P (1987) *Acta Crystallogr B: Struct Sci* 43:440
6. Cheary RW (1986) *Acta Crystallogr B: Struct Sci* 42:229
7. Post JE, Von Dreele RB, Buseck PR (1982) *Acta Crystallogr B: Struct Sci* B38:1056
8. Cheary RW (1987) *Acta Crystallogr B: Struct Sci* 43:28
9. Cheary RW, Kwiatkowska J (1984) *J Nucl Mater* 125:236
10. Smith RI, Hull S, Armstrong AR (1994) In: *The polaris powder diffractometer at Isis*
11. Smith RI, Hull S (1997) *User guide for the polaris powder diffractometer at ISIS, RAL-TR-97-038, Rutherford Appleton Laboratory*
12. Larson AC, Von Dreele RB (2000) *General Structure Analysis System (GSAS), 86–748, Los Alamos National Laboratory Report LAUR*
13. Toby BH (2001) *J Appl Crystallogr* 34:210
14. Mooibroek S, Wasylishen RE, Dickson R, Facey G, Pettitt BA (1986) *J Magn Reson* 66:542
15. Amoureux JP, Fernandez C, Steuernagel S (1996) *J Magn Reson A* 123:116
16. States DJ, Haberkorn RA, Ruben DJ (1982) *J Magn Reson* 48:286
17. Ernst RR, Bodenhausen G, Wokaun A (1987) Oxford
18. Harris RK, Becker ED, de Menezes SMC, Goodfellow R, Granger P (2002) *Solid State Nucl Magn Reson* 22:458
19. Carter ML, Vance ER, Mitchell DRG, Hanna JV, Zhang Z, Loi E (2002) *J Mater Res* 17:2578
20. Hartman JS, Vance ER, Power WP, Hanna JV (1998) *J Mater Res* 13:22
21. Vega AJ (1996) In: Grant DM, Harris RK (eds) *Encyclopedia of nuclear magnetic resonance*. Chichester
22. Kentgens APM (1997) *Geoderma* 80:271
23. McManus J, Ashbrook SE, MacKenzie KJD, Wimperis S (2001) *J Non-Crystalline Solids* 282:278
24. Frydman L, Harwood JS (1995) *J Am Chem Soc* 117:5367
25. Brown SP, Wimperis S (1997) *J Magn Reson* 128:42
26. Bodart PR (1998) *J Magn Reson* 133:207
27. Shannon RD (1976) *Acta Crystallogr A* A32:751
28. Shannon RD, Prewitt CT (1969) *Acta Crystallogr B: Struct Sci* B25:925
29. Sinclair W, McLaughlin GM, Ringwood AE (1980) *Acta Crystallogr B* 36:2913
30. Cheary RW (1991) *Acta Crystallogr B: Struct Sci* 47:325
31. Vogt T, Schweda E, Wustefeld C, Strahle J, Cheetham AK (1989) *J Solid State Chem* 83:61
32. Watanabe M, Fujiki Y, Kanazawa Y, Tsukimura K (1987) *J Solid State Chem* 66:56
33. Pring A, Smith DJ, Jefferson DA (1983) *J Solid State Chem* 46:373
34. Onoda Y, Fujiki Y, Yoshikado S, Ohachi T, Taniguchi I (1986) *Solid State Ionics* 18–9:878
35. Weber HP, Schulz H (1983) *Zeitschrift Fur Kristallographie* 162:232
36. Lumpkin GR, Ribbe PH (1983) *Am Mineral* 68:164
37. Chakoumakos BC (1984) *J Solid State Chem* 53:120